Understanding hydraulic fracture variability through a penny shaped crack model for pre-rupture faults

David Cho, Gary F. Margrave, Shawn Maxwell and Mark Norton

ABSTRACT

A study was conducted to investigate the large variations in the hydraulic fracture behavior in the vicinity of faults. The process of failure was illustrated through laboratory experiments that demonstrate the formation of aligned microcracks throughout the deformation process. Using a penny shaped crack model, associated properties can be computed to investigate the response of media containing a fault that has yet to rupture. The reflectivity response for the detection of pre-rupture faults is discussed in addition to the presentation of an effective stress model for a medium containing aligned penny shaped cracks. Using the effective stress model, the observed variations can be understood from the response of the aligned cracks to a uniform normal traction applied by a pore fluid.

INTRODUCTION

Hydraulic fracture stimulation plays a vital role in the extraction of unconventional energy resources including low permeability hydrocarbon reserves and enhanced geothermal systems. The objective is to create permeable pathways for fluid flow to extract or capture energy from subsurface formations. Issues that arise are often associated with variations in the in-situ stress field over relatively small distances. For example, in the vicinity of faults, variations in the stress field are significant due to mechanical alterations in the rock mass. Upon stimulation, unexpected fracture behaviors could result in addition to fault activation capable of inducing larger than expected seismicity. These issues must be understood to prevent undesirable outcomes including non-containment or the induction of seismicity capable of damaging nearby infrastructure (i.e. Kraft el al., 2009).

The mechanisms that come into play during stimulation are numerous and many are beyond the capacity of existing theories. However, simple models can be constructed to aid in the understanding of the complex phenomenon. In this study, we present a model that attempts to explain the complex fracture behavior observed in the stimulation program associated with an unconventional gas well. This paper stems from the work of Norton et al. (2010) and Maxwell et al. (2011) in the characterization of a tight gas reservoir to understand the mechanisms that control fracture behavior during stimulation. We being with an overview of the work done previously and proceed with the presentation of a micromechanical model that seeks to explain the observed fracture behavior.

BACKGROUND

The work of Norton et al. (2010) and Maxwell et al. (2011) combined microseismic measurements and attributes derived from reflection seismic to investigate the variability in hydraulic fracture response in the Montney shale of NE British Columbia, Canada. Figure 1 shows the microseismicity associated with the stimulation program of three

horizontal wells. Note the events SW of Well A exhibit a NE-SW trend that propagate away from the wellbore and the events along the length of Wells B and C are constrained to a linear region trending NW-SE. In addition, the magnitude of the microseismicity as illustrated by the size of the spheres also exhibits a large spatial variability.

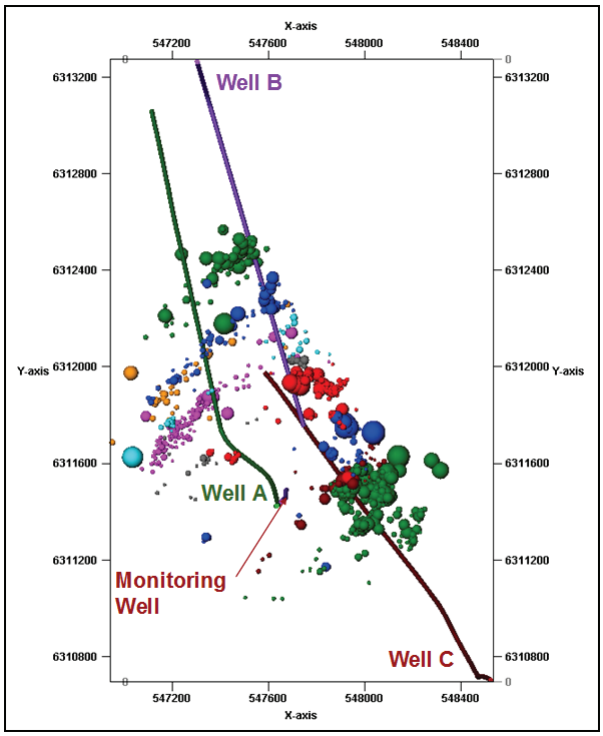

FIG. 1. Map view illustrating the variability in the microseismic response associated with the stimulation of three horizontal wells (Maxwell et al., 2011).

To investigate the large variations in the observed microseismic response, advanced analysis of the microseismicity was implemented to determine the nature of deformation associated with the hydraulic fracture treatment. Calculations of the seismic moment density and *b*-values suggest that the events SW of Well A is consistent with conventional hydraulic fracturing and the events along Wells B and C are consistent with fault activation. In addition, composite amplitude ratios were computed to determine the average failure mechanism associated with the microseismicity. The events SW of Well A is best modeled by a NE-SW strike-slip mechanism in the expected orientation orthogonal to the regional minimum principle stress direction. The events along Wells B and C are best modeled by a NW-SE dip-slip mechanism, which is orthogonal to the expected orientation but is consistent with the regional thrust faults in the area (Maxwell et al., 2011). Figure 2 shows a fault attribute map from the study of Norton et al. (2010) extracted below the reservoir level. A fault is clearly present along the length of Wells B and C, where the associated microseismicity is attributed to the vertical extension of the fault, supporting the notion of fault activation.

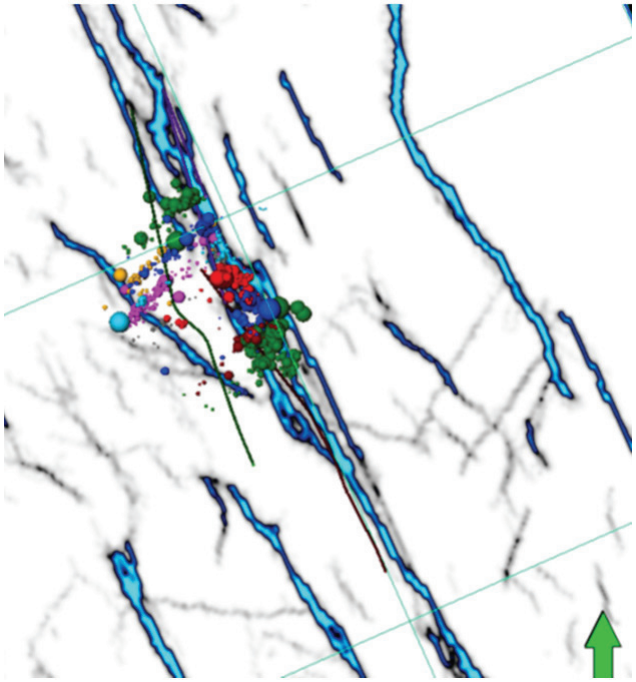

FIG. 2. Microseismic events overlaid on a fault attribute map extracted below the reservoir level.

The results of the study clearly indicate a considerable change in the stress field in the vicinity of faults. Away from the fault, failure occurs under a strike-slip faulting stress regime, where the vertical stress is the intermediate principle stress. In the vicinity of the fault, failure occurs under a thrust faulting stress regime, where the vertical stress is the minimum principle stress. The question then arises as to what is the underlying mechanism that is capable of such considerable changes in the stress field. The following attempts to answer this question by investigating the changes in material properties during the failure process.

FAILURE PROCESS

The stress-strain curve

The process of failure can be modeled in the laboratory in which rock samples can be loaded to investigate the deformation at various points throughout its stress history. Consider a stress-strain curve for a rock subject to uniaxial compression as in Figure 3. The curve can be divided conceptually into three regions where the rock exhibits elastic, ductile and brittle behavior.

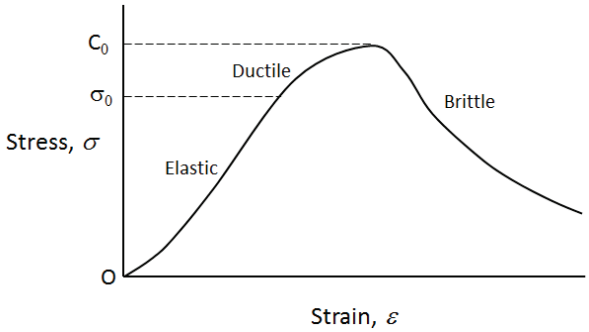

FIG. 3. Stress-strain curve for a rock subject to uniaxial compression.

The elastic regime is characterized by the linear region of the curve. Loading and unloading in this region will follow the same path along the stress-strain curve and will not produce irreversible changes in the structure or material properties of the rock.

The transition from elastic to ductile behavior occurs at a point known as the yield stress, σ_0 of the material. The ductile regime is then characterized by a gradual decrease in the slope of the curve until a value of zero is reached. In this region, the transverse strains begin to grow in magnitude at a much faster rate than the axial strain. This means that an incremental increase in the axial compressive stress results in an incremental increase in the volume, a phenomenon known as dilatancy. The increase in volume under an additional compressive stress can be attributed to the formation and extension of microcracks oriented parallel to the direction of the maximum principle stress. Irreversible changes to the structure and material properties occur throughout this region and successive loading and unloading cycles will follow different paths along the stress-strain curve.

The point at which the slope of the stress-strain curve is zero marks the transition from ductile to brittle behavior and is known as the uniaxial compressive strength, C_0 of the material. The brittle regime is then characterized by a negative slope in the stress-strain curve where failure occurs throughout this region as a continuous process in which the material physically deteriorates.

The in-situ formation of microcracks

Triaxial compression tests are typically performed under the condition of a constant lateral confining stress, where the lateral expansion of the specimen is unrestricted. One can imagine however, that the lateral confining stress in-situ is a function of the surrounding material, which exhibits a finite stiffness. As a rock mass deforms laterally, the adjacent rock would response by increasing the lateral confining stress with increasing lateral strain, therefore inhibiting the localized lateral expansion of the rock mass.

Hallbauer et al. (1973) performed a triaxial compression test that more closely represents the conditions in-situ. Using an annealed copper tube and a fixed fluid volume in a triaxial test cell, they were able to provide stiffness to the confinement of the specimen. Subsequently, the samples were loaded to predetermined points along the

stress-strain curve to investigate the structural changes that occur as a result of loading. Thin sections were then prepared at the various stages of loading to illustrate the mechanical alterations undergone during the deformation process.

Figure 4 illustrates the results of the experiment. The structural changes observed in the specimens consisted of microcracks that formed throughout the deformation process. The orientation of the microcracks is parallel to the direction of the maximum principle stress, which was applied along the axis of the cylindrical samples. In the elastic regime, slight hysteresis occurred where the microcracks were distributed uniformly throughout the sample. In the ductile regime, the density of microcracks increased dramatically as the axial stress approached the ultimate strength of the specimen. Past the yield stress, the distribution of microcracks begins to concentrate near the center of the specimen along a plane and as loading approached the ultimate strength of the specimen, the microcracks coalesce to form a discrete fracture plane.

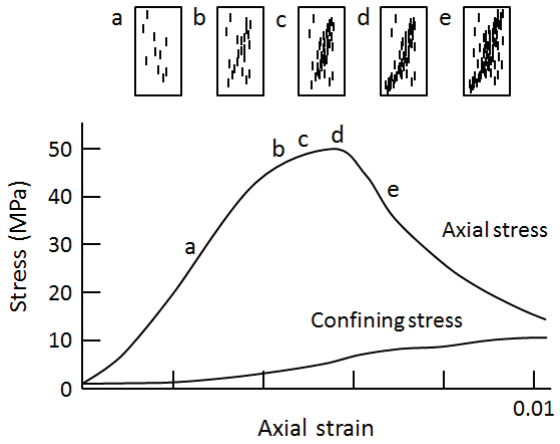

FIG. 4. Structural changes to the specimen at various points along the stress-strain curve (Jaeger et al., 2007).

REFLECTIVITY RESPONSE

The aligned microcracks that form as a result of deformation can be modeled using Hudson's penny shaped crack model. Hudson (1981) derived expressions for the representation of a medium containing aligned penny shaped inclusions as shown in Figure 5.

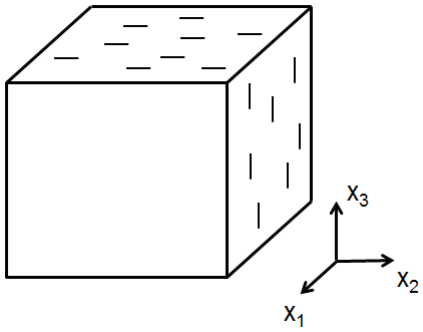

FIG. 5. Aligned penny shaped inclusions in an isotropic background medium.

The effective elastic stiffness parameters of the medium are given by

$$C_{ij}^{(eff)} = C_{ij}^{(0)} + C_{ij}^{(1)} + C_{ij}^{(2)} \tag{1}$$

where $C_{ij}^{(0)}$ represents the elastic stiffness of the isotropic background and $C_{ij}^{(1)}$ and $C_{ij}^{(2)}$ represent the first and second order perturbations due to the inclusion of the penny shaped cracks respectively for i and j running from 1 to 3. For simplicity, we consider the case of dry cracks where the effective elastic stiffness parameters are a function of the crack density, ε and the Lamé parameters, λ and μ.

Consider a medium containing a single interface separating two homogeneous layers. The medium is subsequently loaded in a confined environment to the ductile regime of the stress-strain curve, representing a pre-rupture fault as in Figure 6a. The normal incidence reflection coefficient across the interface is given by

$$R = \frac{V_2^{(eff)}\rho_2 - V_1^{(eff)}\rho_1}{V_2^{(eff)}\rho_2 + V_1^{(eff)}\rho_1} \tag{2}$$

where ρ is the density and $V^{(eff)}$ is the effective vertical P-wave velocity and is given by

$$V^{(eff)} = \sqrt{\frac{C_{33}^{(eff)}}{\rho}} = \sqrt{\frac{1}{\rho}\left(\lambda + 2\mu - \frac{4\lambda^2(\lambda+2\mu)}{3\mu(\lambda+\mu)}\varepsilon\right)}. \tag{3}$$

In the region where microcracks exist, the reflection coefficient changes as a function of the crack density and is illustrated in Figure 6b. The blue curve represents an increase and the red curve represents a decrease in the impedance across the interface.

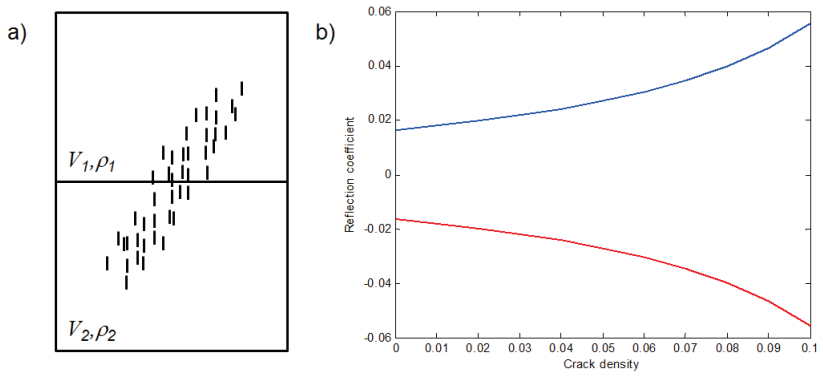

FIG. 6. a) An interface containing aligned microcracks and b) the corresponding reflection coefficients for an increase in impedance (blue) and a decrease in impedance (red) across the interface.

As the crack density increases, the reflection coefficient becomes more positive or negative depending on an increase or decrease in impedance across the interface. Since the geometry associated with the cluster of microcracks forms a planar feature, amplitude changes in the seismic image can be tracked using a pattern recognition algorithm to identify regions where these features exist. However, due to the subtle changes in amplitude across a reflector, noise issues can easily contaminate the response and care must be taken in the interpretation of the results.

AN EFFECTIVE STRESS MODEL FOR PENNY SHAPED CRACKS

Consider an infinitely thin crack in an isotropic homogenous background medium as illustrated by the solid blue line in Figure 7. The crack is subjected to a uniform normal traction, p applied to its faces, as would be the case for the pressure exerted by a pore fluid. Sneddon (1946) derived the displacement for the crack surface in a direction normal to its plane and is given by

$$w(r) = \frac{2(1-\nu)pa}{\pi\mu}\sqrt{1-(r/a)^2}\,, \tag{4}$$

where ν and μ are the Poisson's ratio and shear modulus of the isotropic background medium respectively, a is the radius of the crack and r is the radial distance from the center of the crack in the crack plane. The pressurization of the crack results in an opening displacement that is greatest in the center and zero at the crack edge as illustrated by the dashed blue line in Figure 7.

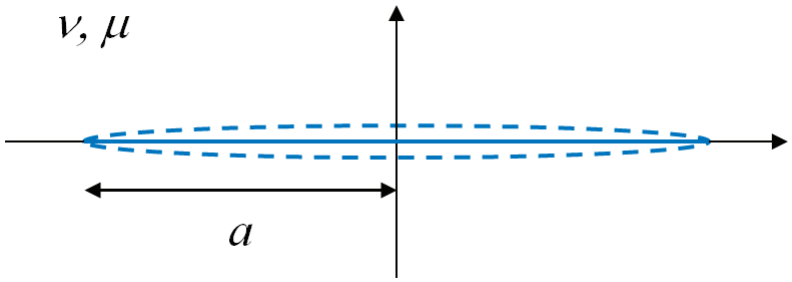

FIG. 7. Schematic for an infinitely thin crack and the associated displacement (dashed line) upon the application of a uniform normal traction.

The excess elastic strain energy due to a pressurized crack can be calculated as in Jaeger et al. (2007) by solving

$$W_{crack} = \frac{1}{2}\int_{2A} pwdA = \int_0^{2\pi}\int_0^a \frac{2(1-\nu)p^2 a}{\pi\mu}\sqrt{1-(r/a)^2}\,rdrd\theta\,, \tag{5}$$

which yields

$$W_{crack} = \frac{4(1-\nu)p^2 a^3}{3\mu}\,. \tag{6}$$

Now consider a medium with a volume, V containing N number of cracks. The resulting excess elastic strain energy density can be obtained by the multiplication of equation 6 by N/V. In addition, using the definition of crack density as given by

$$\varepsilon = \frac{Na^3}{V}, \tag{7}$$

an expression for the excess elastic strain energy density as a function of crack density can be obtained and is given by

$$W = \frac{4(1-\nu)p^2\varepsilon}{3\mu}\,. \tag{8}$$

We seek an expression for the effective stress due to the presence of aligned penny shaped cracks subjected to a pore pressure, p. Assuming that the opening displacement is small, the normal to the crack face lie along a single axis and therefore, the stresses exerted by the pore fluid is unidirectional and only applies normal to the crack face. Differentiation of equation 8 with respect to p then yields the excess strain as a result of the pressurized cracks and is given by

$$e_{ii}^{(excess)} = \frac{\partial W}{\partial p} = \frac{8(1-\nu)p\varepsilon}{3\mu}, \tag{9}$$

where i indicates the direction normal to the crack face. The corresponding excess stress is then given by

$$\sigma_{ii}^{(excess)} = \frac{8E_i(1-\nu)p\varepsilon}{3\mu}, \tag{10}$$

where E_i represents the Young's modulus. Note that E_i is associated with the effective medium as a result of the inclusion of the penny shaped cracks. Since the penny shaped inclusions result in an anisotropic medium, E_i can be calculated using the following relationships,

$$E_1 = \frac{D}{C_{22}^{(eff)}C_{33}^{(eff)} - C_{23}^{(eff)2}},\ E_2 = \frac{D}{C_{11}^{(eff)}C_{33}^{(eff)} - C_{13}^{(eff)2}},\ E_3 = \frac{D}{C_{11}^{(eff)}C_{22}^{(eff)} - C_{12}^{(eff)2}},$$

where

$$D = \det\begin{vmatrix} C_{11}^{(eff)} & C_{12}^{(eff)} & C_{13}^{(eff)} \\ C_{12}^{(eff)} & C_{22}^{(eff)} & C_{23}^{(eff)} \\ C_{13}^{(eff)} & C_{23}^{(eff)} & C_{33}^{(eff)} \end{vmatrix}, \tag{11}$$

depending on the orientation of the cracks. The effective elastic stiffness parameters in equation 11 are then given by the appropriate formulation as given by Hudson (1981) for dry or fluid filled cracks. The resulting effective stress normal to the crack face is then given by

$$\sigma_{ii}^{(eff)} = \sigma_{ii} - \sigma_{ii}^{(excess)} = \sigma_{ii} - \beta p,$$

where

$$\beta = \frac{8E_i(1-\nu)\varepsilon}{3\mu}. \tag{12}$$

The parameter β is analogous to the Biot-Willis parameter, α, which represents the proportion of fluid pressure which will produce the same strains as the total stress (Biot and Willis, 1957). In most porous rocks, the pressure applied inside the pores will result in a smaller strain on the total rock volume as opposed to the same pressure applied on the outside of the volume, therefore α and β will take on values that are typically less than one.

DISCUSSION

Given the above description of the failure process and an effective stress model for penny shaped cracks, we can proceed with the presentation of a model to explain the large variability of the stress field in the stimulated region. During the formation of the thrust faults in the study area, one can imagine that there exists a complete range of rocks that is at the various stages of the deformation process. The area along the length of Wells B and C where fault activation occurred is hypothesized to be loaded to the ductile region of the stress-strain curve, representing a pre-rupture fault. Since the maximum and minimum principle stress directions in a thrust faulting stress regime are horizontal and vertical respectively, the microcracks that form as a result of loading lie in the horizontal plane. Figure 8 shows a model of the medium where the left side represents the intact

rock and the right side represents the pre-rupture fault. Both regions possess spherical pores and the region representing the pre-rupture fault has an additional set of aligned penny shaped cracks. For simplicity, we also assume that the pores and cracks are dry for the following calculations.

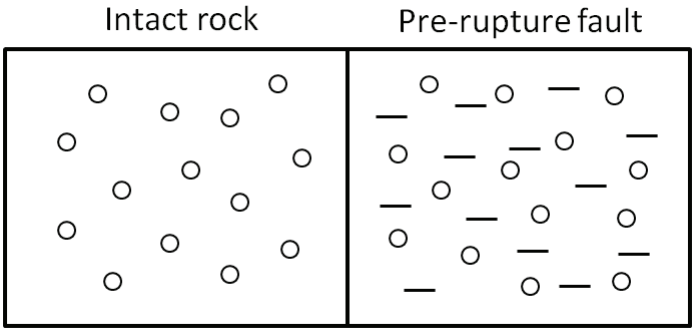

FIG. 8. Model for the intact rock and the pre-rupture fault.

In a strike-slip faulting stress regime, $\sigma_H^{(eff)} > \sigma_V^{(eff)} > \sigma_h^{(eff)}$ and in a thrust faulting stress regime, $\sigma_H^{(eff)} > \sigma_h^{(eff)} > \sigma_V^{(eff)}$, where the subscripts V, H and h denote the vertical and maximum and minimum horizontal stresses respectively. Therefore, we are interested in the relative magnitudes of $\sigma_V^{(eff)}$ and $\sigma_h^{(eff)}$ for the two regions in Figure 8. For the intact rock, the effective vertical stress is given by

$$\sigma_V^{(eff)} = \sigma_V - \alpha p \tag{13}$$

and for the pre-rupture fault, the effective vertical stress is given by

$$\sigma_V^{(eff)} = \sigma_V - (\alpha + \beta) p \,. \tag{14}$$

The effective minimum horizontal stress for both the intact rock and pre-rupture fault is given by

$$\sigma_h^{(eff)} = \sigma_h - \alpha p \,. \tag{15}$$

The Biot-Willis parameter, α, is defined as

$$\alpha = 1 - K^{(eff)} / K \,, \tag{16}$$

where K represents the bulk modulus. The effective bulk modulus can then be calculated using

$$1/K^{(eff)} = C^{(eff)} = C + \phi C_p \,, \tag{17}$$

where C represents the compressibility, ϕ is the porosity and the subscript p denotes the pore compressibility, which is given by

$$C_p = \frac{3}{4\mu}, \tag{18}$$

for spherical pores (Jaeger et al., 2007). We estimate the vertical stress using a pressure gradient of ~25 kPa/m and the minimum horizontal stress from the measured closure stress value of ~23 kPa/m (Maxwell et al., 2011). Average values for the P- and S-wave velocities and density in the Montney was taken to be 4750 m/s, 2800 m/s and 2650 kg/m^3 respectively. In addition, we use a porosity and crack density value of 0.05. The resulting values for α and β are 0.05 and 0.19 respectively. Note the difference in the values of α and β. This is due to the geometry of the pores where the same pressure is applied along a single dimension for β and three dimensions for α. Figure 9 shows the effective vertical and minimum horizontal stress as a function of pore pressure for the intact rock and the pre-rupture fault.

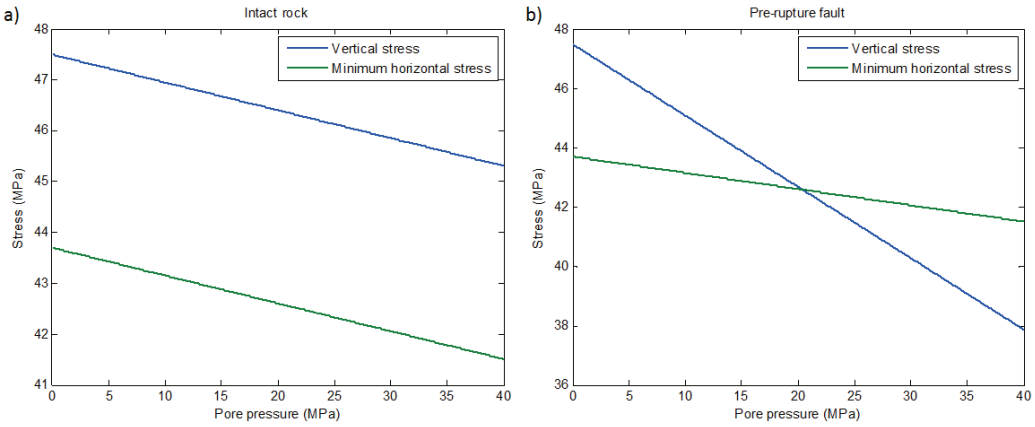

FIG. 9. Effective vertical and minimum horizontal stress for a) the intact rock and b) the pre-rupture fault.

For the intact rock, the effective stresses decrease at a similar rate with increasing pore pressure, therefore remaining in the original strike-slip faulting stress regime. The pre-rupture fault however, has an effective vertical stress that decreases at a faster rate than the effective minimum horizontal stress. Therefore, a crossover from a strike-slip faulting stress regime into a thrust faulting stress regime occurs upon an increase in the pore pressure, resulting in a change in the stress field and the corresponding variations in the microseismic response.

CONCLUSIONS

The proposed effective stress model for aligned pressurized cracks results in an excess stress that acts only in a direction normal to the crack face. Therefore, changes in the stress field due to pore pressure are directional. As opposed to the Biot-Willis parameter, α, which is isotropic and therefore applies to spherical pore geometries, the parameter, β is anisotropic. Therefore, in media where the pore geometry can be approximated by penny shaped cracks such as materials that are loaded to the ductile regime of the stress-strain curve as discussed above or shales where the pore structure is flat due to the alignment of clay platelets, the proposed effective stress model can be used.

REFERENCES

Hallbauer, D. K., Wagner, H., and Cook, N. G. W., 1973, Some observations concerning the microscopic and mechanical behavior of quartzite specimens in stiff triaxial compression tests: Int. J. Rock Mech., 10, 713-26.

Hudson, J. A., 1981, Wave speeds and attenuation of elastic waves in material containing cracks: Geophysical Journal of the Royal Astronomical Society, 64, 133–150.

Jaeger, J. C., Cook, N. W. G., and Zimmerman, R. W., 2007, Fundamentals of Rock Mechanics, 4th ed. Chapman and Hall.

Kraft et al., 2009, Enhanced Geothermal Systems: Mitigating Risk in Urban Areas, EOS, AGU, Vol. 90, No. 32, P. 273.

Maxwell, S. C., Cho, D., Pope, T., Jones, M., Cipolla, C., Mack, M., Henery, F., Norton, M., 2011, Enhanced reservoir characterization using hydraulic fracture microseismicity: SPE Hydraulic Fracturing Technology Conference and Exhibition, The Woodlands, Texas, SPE 140449.

Norton, M., Hovdebo, W., Cho, D., Jones, M., and Maxwell, S., 2010, Surface seismic to microseismic: An integrated case study from exploration to completion in the Montney Shale, NE British Columbia, Canada, SEG Expanded Abstracts.

Sneddon, I. N., 1946, The distribution of stress in the neighborhood of a crack in an elastic solid: Proc. Roy. Soc. Lond. Ser. A, 187, 229-60.